Title: CFD modelling of a mixing chamber for the realisation of functionally graded scaffolds

Author: G. Mattei G. Vozzi

PII: S0098-1354(15)00282-3
DOI: http://dx.doi.org/doi:10.1016/j.compchemeng.2015.08.021
Reference: CACE 5272

To appear in: *Computers and Chemical Engineering*

Received date: 20-6-2014
Revised date: 11-6-2015
Accepted date: 21-8-2015

Please cite this article as: Mattei, G., and Vozzi, G.,CFD modelling of a mixing chamber for the realisation of functionally graded scaffolds, *Computers and Chemical Engineering* (2015), http://dx.doi.org/10.1016/j.compchemeng.2015.08.021

Highlights

- We model hydroxyapatite particle mixing within a gelatin solution in a stirred tank
- The stirred tank geometry and configuration allow to obtain homogeneous suspensions
- Discrete or continuous graded bone scaffolds can be obtained from these suspensions
- Results help to design small stirred tanks for automated bone scaffold fabrication

CFD modelling of a mixing chamber for the realisation of functionally graded scaffolds

G. Mattei [a,*] and G. Vozzi [a,b]

[a] Research Centre "E. Piaggio", University of Pisa, Largo Lucio Lazzarino 1, 56122 Pisa, Italy

[b] Department of Information Engineering, University of Pisa, Via G. Caruso 16, 56122 Pisa, Italy

[*]Corresponding Author

Address: Research Centre "E. Piaggio", University of Pisa, Largo Lucio Lazzarino 1, 56122 Pisa, Italy

Tel: +39 050 2217056

Fax: +39 050 2217051

E-mail: giorgio.mattei@centropiaggio.unipi.it

Abstract

Biological tissues are characterised by spatially distributed gradients, intricately linked with functions. It widely accepted that ideal tissue engineered scaffolds should exhibit similar functional gradients to promote successful tissue regeneration. Focusing on bone, in previous work we proposed simple methods to obtain osteochondral functionally graded scaffolds (FGSs), starting from homogeneous suspensions of hydroxyapatite (HA) particles in gelatin solutions. With the main aim of developing an automated device to fabricate FGSs, this work is focused on designing a stirred tank to obtain homogeneous HA-gelatin suspensions. The HA particles transport within the gelatin solution was investigated through computational fluid dynamics (CFD) modelling. First, the steady-state flow field was solved for the continuous phase only. Then, it was used as a starting point for solving the multi-phase transient simulation. CFD results showed that the proposed tank geometry and setup allow for obtaining a homogeneous suspension of HA micro-particles within the gelatin solution.

Keywords: Computational fluid dynamics; stirred tank; particle suspension; functionally graded scaffolds; tissue engineering

1. Introduction

Biologically inspired approaches have been widely accepted in designing better implants as well as in manufacturing artificial tissues. In general, tissues are characterised by hierarchical structures with spatially distributed gradients of properties and composition, that are intimately linked with functions (Miyamoto, Kaysser, Rabin, Kawasaki, & Ford, 1999). For instance, bone

tissue, with its stiff external region (i.e. cortical bone) gradually changing to a porous spongy honeycombed internal one (i.e. cancellous bone), demonstrates how the functional gradation has been used in biological adaptation to optimise the material response to external loadings. The current consensus is that an ideal tissue-engineered scaffold should recapitulate most of the native tissue characteristics to provide cells with an optimal micro-environment promoting cell growth and differentiation. Therefore, functionally graded scaffolds (FGSs) are critical for the successful engineering of biological tissues. A variety of manufacturing methods for the fabrication of FGSs have been proposed, including multiple tape casting (Werner, Linner-Krčmar, Friess, & Greil, 2002), injection molding (Zhang, Chang, Lu, Lin, & Ning, 2007), multiple and differentiated impregnations (A Tampieri, Celotti, Sprio, Delcogliano, & Franzese, 2001), modified sponge replication (Hsu, Turner, & Miles, 2007) and freeze-casting (Macchetta, Turner, & Bowen, 2009). However, the development of new manufacturing methods that can tightly control the gradient of properties in a cost-effective way is still a challenge (Miao & Sun, 2009). Focusing on bone tissue, which is mainly composed by hydroxyapatite (HA) and collagen (Col), we have recently investigated simple methods to obtain osteochondral FGSs with either discrete or continuous gradient profiles. In particular, discrete FGSs were prepared by stacking homogeneous HA-gelatin (HA/Gel) suspensions with different HA/Gel weight ratios (Jelen et al., 2013), while continuous FGSs were obtained using the gravitational sedimentation of HA particles that occurs during the controlled cross-linking of homogeneous HA/Gel suspensions (Mattei, Tirella, & Ahluwalia, 2012). These methods are very suited for developing an automated device to realise either discrete or continuous FGSs for tissue engineering applications. Mechanical agitation is widely used in industrial processes involving solid-liquid

flows, with the typical requirement of suspending the solid phase for dissolution, enhanced reaction, or to obtain uniform suspensions, as in our case. Among the various approaches to provide mechanical agitation (e.g. sonication, vortexing, stirring, etc.) we chose to suspend particles through mixing in a small stirred tank. Understanding the fluid dynamics in the stirred tank is critical to properly design a mixing chamber that ensures a homogeneous suspension of HA micro-particles (secondary solid discrete phase) within the gelatin solution (primary liquid phase) prior to be transferred into a mold. Multi-phase computational fluid dynamics (CFD) modelling significantly helps in designing the stirred tank, limiting the expensive and time-consuming *trial-and-error* experimental approach. CFD modelling has become a powerful tool for the prediction of flow fields and mixing in stirred tanks, being very helpful for estimating important process parameters such as the homogenisation time (t_H, i.e. the time required to achieve a fully-mixed state) and the requested power input. Several approaches to modelling solids transport were proposed, including both Lagrangian and Eulerian techniques. The Eulerian multiphase model is of particular interest, since it uses separate sets of Navier-Stokes equations for the liquid and the solids (or granular) phases, coupling the interactions between them. Using Eulerian-Eulerian models, Micale et al. predicted particle distribution at low particle concentrations in single and multiple impeller stirred vessels (Micale, Montante, Grisafi, Brucato, & Godfrey, 2000). Even though their results were in good agreement with experimental axial measurements of solids concentration, they used correction factors to fit the numerical predictions to experimental data, concluding that improved single-phase simulations and incorporation of the so-called four-way interactions (i.e. fluid-particle, particle-fluid, particle-particle and particle-turbulence) would enhance model applicability and reliability. The Eulerian

Granular Multiphase (EGM) model accounts for the four-way coupling between and within phases, providing a fully predictive solution of the solids transport in the stirred tank. The strongly coupled momentum equations of granular and liquid phases require a transient solution (Massah & Oshinowo, 2000).

In this paper, multiphase CFD modelling is used to study the distribution of HA micro-particles in a gelatin solution at 40 °C (modelled as water) within a stirred tank. In particular, the transient start-up of a purposely designed mixing tank driven by a 4 blade radial paddle (RP4) is presented, considering the HA secondary phase initially located at the bottom of the tank, at a given homogenous concentration. The rest of the domain is composed of HA-free gelatin solution. This case is of particular interest for the realisation of discrete FGS by stacking different homogeneous HA/Gel layers, as we proposed. In fact, the FGS fabrication can be automated by designing a device which integrates and controls a small stirred tank with an actuated bottom that can be opened and closed to transfer the HA/Gel suspension to an underlying mold. In particular, first a homogeneous HA-rich suspension is prepared in the stirred tank and partially transferred into the mold, realising the subchondral bony layer of the osteochondral FGS. Then, the remaining HA/Gel mixture in the stirred tank is sequentially diluted with a HA-free gelatin solution, obtaining less HA-rich suspensions for intermediate FGS layers. The latter are sequentially cast into the mold towards a HA-free region, resembling the cartilaginous layer. The stirred tank should be properly designed to guarantee a homogeneous particle suspension after each dilution. The pre-processor MixSim 2.0 (Fluent Inc., USA) was used to create the computational grid with multiple reference frames (MRF), while numerical calculations in the agitated vessel were solved using ANSYS FLUENT (Ansys Inc., USA).

Computations were performed assuming a standard k-ε model of turbulence and modelling the multiphase flow using the EGM. First the steady-state flow field was solved for the continuous phase only (i.e. gelatin solution), and then used as a starting point for the multi-phase transient simulation. Steady-state flow field in the stirred tank and time-varying concentrations of HA particles obtained from the numerical simulations will be presented and discussed.

2. Material and methods

2.1. Experimental problem description

According to the experimental protocols showed in (Jelen et al., 2013; Mattei et al., 2012), a mixing chamber with a volume of about 2 mL was designed and modelled to prepare the homogeneous HA/Gel suspension to realise discrete or continuous FGS. The stirred tank has a flat bottom and an inner diameter of T = 14 mm (Fig. 1). The liquid level is $T = H$ = 14 mm. The off-bottom clearance is $C = T/4$ = 3.5 mm. The custom made centric shaft has a diameter of 2 mm and ends with an integrated 4 blade radial paddle impeller (RP4). The latter moves in clockwise direction at a constant rotational speed N = 240 rpm, chosen on the basis of experimental tests previously performed in our laboratory with a similar setup. The RP4 impeller has a diameter of D = 9 mm ~ 0.64 T, in agreement to the typical dimensions reported in the literature, i.e.0.5-0.8 T (Inglezakis & Poulopoulos, 2006). Blades are B = 3 mm in height and 1 mm in thickness. The 2 mm cylindrical core at the centre of the impeller (Fig. 1b) guarantees a geometrical continuity with the shaft, enhancing the overall mechanical stability of the rotating

elements and improving the fluid dynamics at the blades crossing point, avoiding any zone of stagnation, with respect to sharp perpendicular angles.

According to the geometry described, the resultant volume of liquid within the stirred tank was 2.0742 mL. Since we used the multiple reference frame (MRF) approach for CFD calculations (section 4), this volume was divided in two domains: a rotating zone around the impeller (*radial paddle*) and an external region (*continuum*) with no assigned motion. Considering the sequential dilution approach to obtain discrete FGSs previously described, we studied the transient mixing between a HA-rich gelatin suspension initially located in the *radial paddle* region only and a HA-free gelatin solution located in the rest of the stirred-tank liquid volume (i.e. *continuum* zone). The primary liquid phase was represented by a 5% w/v gelatin solution at 40°C, here modelled as water (density, 1 g/cm^3; viscosity, 1 cP). The volume fraction of HA micro-particles (density, 3.157 g/cm^3; average diameter, 10 μm) in the *radial paddle* region was set to 0.037, resembling the remaining portion of a 70/30 HA/Gel suspension, previously prepared for the bony layer of the ostechondral FGS (Mattei et al., 2012; Anna Tampieri et al., 2008).

2.2. CFD calculations

The software package from Fluent Inc. was used for the CFD simulations. In particular, MixSim 2.0, a specialised pre-processor for mixing applications, was used for defining the mixing tank configuration and for generating the computational grid. The model was then solved using ANSYS FLUENT.

2.2.1. Multiphase flow model

The multiphase model for CFD calculations is commonly selected using two parameters: i) the average inter-particle space (L/d_s) and ii) the Stokes number (*St*). The former can be estimated according to Crowe et al. (Crowe, Sommerfeld, & Tsuji, 1998). In the *worst* case of higher HA volume fraction (i.e. α_{HA} = 0.037), a value of L/d_s = 2.42 is obtained, where d_s represents the HA particle diameter equal to 10 μm. The Stokes number is defined as the ratio between the particulate relaxation time and the system response time, $St = \tau_s/t_{sys}$, where $\tau_s = \frac{\rho_s d_s^2}{18\mu_l}$ and t_{sys} is based on the characteristic length (L_{sys}) and the characteristic velocity (V_{sys}) of the system under investigation: $t_{sys} = L_{sys}/V_{sys}$. Considering $L_{sys} = T$ = 14 mm (i.e. tank diameter) and V_{sys} = 2π·(*N/60*)·(*D/2*) = 0.113 m/s (i.e. the velocity at the extremity of a radial paddle blade, equal to the maximum velocity in the stirred vessel) we obtain $St = 1.41 \cdot 10^{-4}$. In case of low particulate loading (i.e. $L/d_s > 1$) and very low Stokes number ($St \ll 1$) the coupling between the phases is one-way, i.e. the fluid carrier influences the particles via drag and turbulence, but the particles have no influence on the fluid carrier.

However, in this work we chose the Eulerian modelling approach, the most rigorous among the multiphase models, to model multiple separate, yet interacting phases. It is based on a multi-fluid approach and treats the multiple phases as interpenetrating continuums: a single pressure is shared by all phases, while a separate set of continuity and momentum equations is solved for

each phase. The interaction between phases is modelled through the momentum exchange terms and includes the drag exerted by the continuous phase on the dispersed phase. Solid-phase stresses in the Eulerian granular multiphase (EGM) model are derived making an analogy between the random particle motion (arising from particle-particle collisions) and the thermal motion of molecules in a gas (Dimitri Gidaspow, 1994). Therefore, a stress tensor based on the kinetic theory for granular flow is included in the granular momentum equation. The kinetic energy associated with the particle velocity fluctuations is represented by a "pseudo-thermal" or granular temperature, which is proportional to the mean square of the random motion of particles, hence an additional transport equation for granular temperature (or solids fluctuating energy) is modelled.

2.2.2. EGM model: fundamental equations

Fundamental equations used to solve the EGM model are presented below in their general form, where ***q*** refers to the analysed phase, while ***p*** represents one of the *n* phases of the model. Symbols used are listed in the Nomenclature section at the end of the manuscript.

The mass conservation or continuity equation for a phase ***q*** is:

$$\frac{\partial}{\partial t}(\alpha_q \rho_q) + \nabla \cdot (\alpha_q \rho_q \vec{v}_q) = \sum_{p=1}^{n} (\dot{m}_{pq} - \dot{m}_{qp}) + S_q \qquad (1)$$

Since no mass transfer occurs in our system and as no species sources are present, both mass transfer terms ($\dot{m}_{pq}$ and $\dot{m}_{qp}$) and source term S_q are null within the presented mixing model.

The momentum balance for a phase ***q*** can be expressed as:

$$\frac{\partial}{\partial t}(\alpha_q \rho_q \vec{v}_q) + \nabla \cdot (\alpha_q \rho_q \vec{v}_q \vec{v}_q) = -\alpha_q \nabla p + \nabla \cdot \overline{\overline{\tau}}_q + \alpha_q \rho_q \vec{g} + \sum_{p=1}^{n} (\vec{R}_{pq} + \dot{m}_{pq} \vec{v}_{pq} - \dot{m}_{qp} \vec{v}_{qp}) + (\vec{F}_q + \vec{F}_{lift,q} + \vec{F}_{vm,q}) \quad (2)$$

where $\vec{v}_{pq}$ is the interphase velocity related to the mass transfer term $\dot{m}_{pq}$, hence null, and $\overline{\overline{\tau}}_q$ represents the $\boldsymbol{q}^{\text{th}}$ phase stress-strain tensor expressed below (Eq. 3).

$$\overline{\overline{\tau}}_q = \alpha_q \mu_q (\nabla \vec{v}_q + \nabla \vec{v}_q^{\,T}) + \alpha_q (\lambda_q - \frac{2}{3}\mu_q) \nabla \cdot \vec{v}_q \overline{\overline{I}} \quad (3)$$

The lift force ($\vec{F}_{lift,q}$) acts on a particle mainly due to velocity gradients in the primary-phase flow field. Since it is generally more relevant for larger particles and rather insignificant compared to the drag force, $\vec{F}_{lift,q}$ is neglected in the computational model. The *virtual mass effect* (VME) occurs when a secondary phase ***p*** accelerates relative to the primary fluid phase ***q***, as the inertia of the primary-phase mass encountered by accelerating particles exerts a *virtual mass force* on the particles, represented by $\vec{F}_{vm,q}$ in Eq. 2. The VME effect is not considered in the model, since it is significant only when the secondary phase density is much smaller than that of the primary phase.

EGM model equations must be closed with appropriate expressions for the interphase force ($\vec{R}_{pq}$ in Eq. 2), depending on friction, pressure, cohesion, and other effects, and subjected to the conditions that $\vec{R}_{pq} = -\vec{R}_{qp}$ and $\vec{R}_{qq} = 0$. ANSYS FLUENT models this force using a simple interaction (Eq. 4), where $K_{pq} (= K_{qp})$ represents the interphase momentum exchange coefficient.

$$\sum_{p=1}^{n} \vec{R}_{pq} = \sum_{p=1}^{n} K_{pq}(\vec{v}_p - \vec{v}_q) \quad (4)$$

Generally, the momentum exchange between phases in granular flows depends on fluid-fluid, fluid-solid and solid-solid exchange coefficients respectively termed K_{ll}, K_{sl} and K_{ls}. Since the modelled system consists only of a primary liquid phase (gelatin solution) and a secondary granular phase (HA particles), the fluid-fluid exchange coefficient can be neglected. The Gidaspow model (D. Gidaspow, Bezburuah, & Ding, 1992) is chosen for the fluid-solid exchange coefficient, while the solid-solid exchange coefficient between particles is modelled according to Syamlal et al. (Syamlal, 1987).

The granular-phase momentum equation contains a solid pressure term composed of a kinetic term and a second term due to particle collisions. The Lun et al. formulation (default settings in ANSYS FLUENT) is chosen to compute solids pressure. The probability of collisions between particles changes when the solid granular phase becomes dense. This phenomenon is modelled through a correction factor called radial distribution function. Since our mixing problem involves only a single solid phase, the latter is represented according to Lun et al. (Ogawa, Umemura, & Oshima, 1980).

The maximum volume fraction of randomly packed solid objects ($\alpha_{s,\max}$) is defined using the packing limit, an important empirical parameter with no precise geometric definition: theoretically, it depends on the number and the diameter of particles dispersed within a given volume. In case of mono-dispersed spherical particles, random close packing cannot exceed a

density limit of 0.634 (Song, Wang, & Makse, 2008). In our model, this theoretical (default) value is considered for the packing limit.

Shear and bulk viscosities arising from particles momentum exchange (due to translation and collision) are contained in the solid stress tensor. The solid shear viscosity is the sum of collisional, kinetic and frictional components. The granular viscosity model of Syamlal and O'Brien is adopted for the collisional and kinetic parts (Syamlal, Rogers, & O'Brien, 1993), while the frictional component is neglected in the numerical model, since it accounts for the generation of frictional stresses between particles, which is relevant only for dense flow at low shear. The resistance of the granular particles to compression and expansion is accounted in the solids bulk viscosity term, here modelled according to Lun et al. (Lun, Savage, Jeffrey, & Chepurniy, 1984).

The granular temperature is solved using an algebraic formulation (default settings in ANSYS FLUENT), thus neglecting convection and diffusion in the transport equation. Surface tension between fluid and granular solid phase is not considered in the model. Turbulence in the liquid phase is modelled using the standard k-ε model, while turbulence generation by the secondary granular phase is neglected.

2.3. Numerical procedure and solution strategy

The pre-processor MixSim 2.0 (Fluent Inc., USA) is used to create the computational grid with multiple reference frames (MRF), defining the geometry of the vessel, type of the impeller, geometry and density of the numerical grid and part of the boundary conditions. An unstructured

3D computational grid mainly composed of tetrahedral cells is generated. The assignment of grid density can be specified in different parts of the vessel, setting the initial mesh size or the size of a grid cell on the basis of the impeller, shaft, baffles and other components used in the tank. Initial mesh sizes are kept at default software values. The impeller motion is modelled using the multiple reference frame (MRF) approach. The vessel is divided in two parts, a moving frame around the impeller (*radial paddle*) and a stationary frame (*continuum*) attached to the vessel wall. The dimensions of the rotating fluid zone for MRF are evaluated on the basis of the impeller geometry using default expressions provided by MixSim 2.0. The computational grid obtained is shown in Fig. 2: it has 75053 cells, characterised by an average *skewness* of 0.34, thus being an excellent grid for 3D flow problems (Sun, 2007).

Governing equations were solved numerically using ANSYS FLUENT. No slip boundary conditions are applied on all tank walls and shaft with the latter moving at the prescribed rotational velocity of N = 240 rpm. The free surface of the suspension is characterised by zero gradients of velocity and all other variables. Since the shear stress is null, it can be interpreted as a zero-shear slip wall, hence it is modelled with symmetry boundary conditions. The impeller motion at N = 240 rpm is modelled using the MRF approach. Materials properties are set as outlined in Section 2 and gravity is fixed at 9.81 m/s^2. After obtaining the continuous liquid phase flow field, HA particles are patched only in the *radial paddle* region, at a volume fraction of 0.037, as discussed in Section 2. Then the time-dependent HA-gelatin mixing problem is solved using the EGM model. The starting time-step is 0.005 s, then it is increased to 0.01 s after solving the first second of the transient. CFD calculations are performed until a steady-state solution is obtained, i.e. after the homogenisation time, t_H, determined using the coefficient of

variation (CoV) of the HA volume fraction within the stirred tank (Coroneo, Montante, Paglianti, & Magelli, 2011). The CoV(t) is defined as the ratio of the standard deviation of HA volume fraction at time t to its final equilibrium value (equal to 0.0115 for the modelled problem). The homogenisation time (t_H) is taken as the instant at which the CoV becomes stable in time and below 0.05, according to many published works using the t_{95}, i.e. the mixing time after which the concentration of a species has reached and remains within a 5% range of the final equilibrium value (Moštěk, Kukukova, Jahoda, & Macho\vn, 2005; Ochieng, Onyango, & Kiriamiti, n.d.).

3. Results and discussion

The flow field within the stirred tank generated by the RP4 impeller rotation at N = 240 rpm is shown in Fig. 3. Velocity profiles at the axial cross-sections of the vessel passing in the middle of the RP4 blades (θ = 0°) and through the blades (θ = 45°) are shown in Fig. 3a and 3b, respectively. When the flow impacts on the tank wall, it splits up into two parts and changes the direction. Then, the split flow returns to impeller region and accelerated again. Repeating this process, two circulation loops of different directions were generated in the upper and lower part of the tank, respectively. Vector plots clearly highlight these loops, which are indispensable for suspending HA particles within the stirred tank. Radial velocity profiles for two sections parallel to the tank bottom, located at 3.5 mm and 10.5 mm above it, are presented in Fig. 3c. The fluid flow is highest near the impeller, reaching its maximum velocity at the tip of the RP4 blades (equal to $2\pi\cdot(N/60)\cdot(D/2)$ = 0.113 m/s), while it becomes relatively low near the free surface.

The distribution of HA volume fraction versus time while stirring is shown in Fig. 4 using contour plots at the same axial cross-sections chosen for the velocity field, i.e. $\theta = 0°$ and $\theta = 45°$. Moreover, the axial distributions of the dimensionless HA volume fraction over time (defined as $\alpha_{HA}(z,t)/\alpha_{HA,eq}$, with $\alpha_{HA,eq} = 0.0115$) evaluated for the dimensionless radial coordinate $r^* = r/R = 0.5$ ($R = T/2 = 7$ mm) belonging to the $\theta = 0°$ axial cross-section plane are shown in Fig. 5. At time 0, the HA was homogeneously suspended in the *radial paddle* region only, at the prescribed volume fraction of 0.037. Then, the two circulation loops generated by the RP4 impeller agitation, draw the gelatin primary phase down to the HA-rich lower region of the vessel. To compensate this, HA particles start to rise up, mixing in an ever-increasing volume of HA-free gelatin solution with time. As a result, the maximum volume fraction of HA decreases with time while stirring, until an almost homogenous HA distribution is reached within the vessel after the homogenisation time t_H.

To estimate the homogenisation time, the coefficient of variation (CoV) of the HA volume fraction is calculated considering values computed for the whole stirred tank volume, thus being a better indicator of the suspension homogeneity with respect to considering a point, a line or a surface only. The CoV versus mixing time is shown in Fig. 6.

According to the adopted definition, the homogenisation time can be taken as $t_H = 50$ s, in correspondence to which the CoV value is equal to 0.02, demonstrating that HA particles are almost homogeneously suspended within the stirred tank. Suspension quality (or homogeneity) can be evaluated as 1 – CoV, with 1 representing a theoretically perfect homogeneous suspension (i.e. particle volume fraction independent of the position within the vessel). The

suspension homogeneity for the modelled problem is 0.98, obtained after 50 s of mixing, and did not change by increasing the mixing time, thus confirming that a stable steady state is reached after the t_H, as expected.

4. Conclusions

The mixing of HA micro-particles within a gelatin solution in a custom stirred tank has been investigated through CFD modelling, with the main aim of designing the latter to obtain homogenous HA-gelatin suspensions for fabricating either discrete or continuous osteochondral FGSs. The tank geometry and experimental configuration as well as multi-phase CFD model setup have been described in detail throughout the manuscript. First, only the continuous fluid phase (i.e. gelatin solution) has been considered in the CFD model for solving the steady-state flow field. Then, the initial distribution of HA particles has been defined and the HA-gelatin mixing investigated by solving a time-dependent multi-phase CFD model. Computational results showed that a homogeneous HA-gelatin suspension was obtained after 50 s mixing at a rotational speed of 240 rpm.

In general, this modelling framework can be used to simulate every mixing problem between suspensions with different homogeneous initial particle concentrations. For the sake of easiness in setting-up the CFD model, only two suspensions have been considered in the present work, patching the initial particle distribution in one of the two region requested for solving the single-phase fluid flow within the stirred tank. However, more complex models can be implemented by defining the requested number of domains (> 2, in general) for both setting-up the stirring fluid-

dynamic problem and patching the initial particle distribution, while generating the stirred tank computational grid.

Nomenclature

Symbols are listed in order of appearance within equations shown in the paper.

α_q	$\boldsymbol{q^{th}}$ phase volume fraction
ρ_q	$\boldsymbol{q^{th}}$ phase density
$\vec{v}_q$	$\boldsymbol{q^{th}}$ phase velocity
$\dot{m}_{pq}$	mass transfer from phase $\boldsymbol{p}$ to phase $\boldsymbol{q}$
S_q	$\boldsymbol{q^{th}}$ phase source term
p	pressure (shared by all phases)
$\overline{\overline{\tau}}_q$	$\boldsymbol{q^{th}}$ phase stress-strain tensor
$\vec{g}$	acceleration due to gravity
$\vec{R}_{pq}$	interphase force
$\vec{v}_{pq}$	interphase velocity
$\vec{F}_q$	external body force
$\vec{F}_{lift,q}$	lift force

1	$\vec{F}_{vm,q}$	virtual mass force
2	μ_q	$\boldsymbol{q^{th}}$ phase shear viscosity
3	λ_q	$\boldsymbol{q^{th}}$ phase bulk viscosity
4	K_{pq}	interphase momentum exchange coefficient
5	$\bar{\bar{I}}$	identity tensor
6	d_s	$\boldsymbol{s^{th}}$ solid phase particle diameter

References

Coroneo, M., Montante, G., Paglianti, A., & Magelli, F. (2011). CFD prediction of fluid flow and mixing in stirred tanks: Numerical issues about the RANS simulations. *Computers & Chemical Engineering*, *35*(10), 1959–1968. doi:10.1016/j.compchemeng.2010.12.007

Crowe, C. C. T., Sommerfeld, M., & Tsuji, Y. (1998). *Multiphase Flows with Droplets and Particles Flows*.

Gidaspow, D. (1994). *Multiphase Flow and Fluidization: Continuum and Kinetic Theory Descriptions*. Boston, MA: Academic Press Inc.

Gidaspow, D., Bezburuah, R., & Ding, J. (1992). Hydrodynamics of circulating fluidized beds: Kinetic theory approach. In *In Fluidization VII, Proceedings of the 7th Engineering Foundation Conference on Fluidization* (pp. 75–82).

Hsu, Y. H., Turner, I. G., & Miles, A. W. (2007). Fabrication of porous bioceramics with porosity gradients similar to the bimodal structure of cortical and cancellous bone. *Journal of Materials Science. Materials in Medicine*, *18*(12), 2251–6. doi:10.1007/s10856-007-3126-2

Inglezakis, V. J., & Poulopoulos, S. G. (2006). *Adsorption, ion exchange and catalysis: design of operations and environmental applications*. *null* (Vol. null). Elsevier. doi:10.1016/B978-044452783-7/50003

Jelen, C., Mattei, G., Montemurro, F., De Maria, C., Mattioli-Belmonte, M., & Vozzi, G. (2013). Bone scaffolds with homogeneous and discrete gradient mechanical properties. *Materials Science and Engineering: C*, *33*(1), 28–36. doi:10.1016/j.msec.2012.07.046

Lun, C. K. K., Savage, S. B., Jeffrey, D. J., & Chepurniy, N. (1984). Kinetic theories for granular flow: inelastic particles in Couette flow and slightly inelastic particles in a general flowfield. *Journal of Fluid Mechanics*, *140*, 223–256. doi:10.1017/S0022112084000586

Macchetta, A., Turner, I. G., & Bowen, C. R. (2009). Fabrication of HA/TCP scaffolds with a graded and porous structure using a camphene-based freeze-casting method. *Acta Biomaterialia*, *5*(4), 1319–27. doi:10.1016/j.actbio.2008.11.009

Massah, H., & Oshinowo, L. (2000). Super models. *Chemical Engineer*, (710), 20–22.

Mattei, G., Tirella, A., & Ahluwalia, A. (2012). Functionally Graded Materials (FGMs) with Predictable and Controlled Gradient Profiles: Computational Modelling and Realisation. *CMES: Computer Modeling in Engineering & Sciences*, *87*(6), 483–504. doi:10.3970/cmes.2012.087.483

Miao, X., & Sun, D. (2009). Graded/Gradient Porous Biomaterials. *Materials*, *3*(1), 26–47. doi:10.3390/ma3010026

Micale, G., Montante, G., Grisafi, F., Brucato, A., & Godfrey, J. (2000). CFD Simulation of Particle Distribution in Stirred Vessels. *Chemical Engineering Research and Design*, *78*(3), 435–444. doi:10.1205/026387600527338

Miyamoto, Y., Kaysser, W. A., Rabin, B. H., Kawasaki, A., & Ford, R. G. (1999). *Functionally Graded Materials: Design, Processing and Applications* (pp. 7–28). Kluwer Academic Publishers.

Moštěk, M., Kukukova, A., Jahoda, M., & Macho\vn, V. (2005). Comparison of different techniques for modelling of flow field and homogenization in stirred vessels. *Chem. Pap*, *59*(6a), 380–385.

Ochieng, A., Onyango, M., & Kiriamiti, K. (n.d.). Experimental measurement and computational fluid dynamics simulation of mixing in a stirred tank: a review. *South African Journal of Science*, *105*(11-12), 421–426. doi:10.4102/sajs.v105i11/12.139

Ogawa, S., Umemura, A., & Oshima, N. (1980). On the equations of fully fluidized granular materials. *Zeitschrift Für Angewandte Mathematik Und Physik ZAMP*, *31*(4), 483–493. doi:10.1007/BF01590859

Song, C., Wang, P., & Makse, H. A. (2008). A phase diagram for jammed matter. *Nature*, *453*(7195), 629–32. doi:10.1038/nature06981

Sun, D.-W. (2007). *Computational fluid dynamics in food processing*. CRC press.

Syamlal, M. (1987). The particle-particle drag term in a multiparticle model of fluidization. *National Technical Information Service*.

Syamlal, M., Rogers, W., & O'Brien, T. J. (1993). *MFIX documentation: volume I, Theory Guide*. *National Technical Information Service*. Springfield, VA. DOE/METC-9411004, NTIS/DE9400087.

Tampieri, A., Celotti, G., Sprio, S., Delcogliano, A., & Franzese, S. (2001). Porosity-graded hydroxyapatite ceramics to replace natural bone. *Biomaterials*, *22*(11), 1365–70.

Tampieri, A., Sandri, M., Landi, E., Pressato, D., Francioli, S., Quarto, R., & Martin, I. (2008). Design of graded biomimetic osteochondral composite scaffolds. *Biomaterials*, *29*(26), 3539–46. doi:10.1016/j.biomaterials.2008.05.008

Werner, J., Linner-Krčmar, B., Friess, W., & Greil, P. (2002). Mechanical properties and in vitro cell compatibility of hydroxyapatite ceramics with graded pore structure. *Biomaterials*, *23*(21), 4285–4294. doi:10.1016/S0142-9612(02)00191-6

Zhang, F., Chang, J., Lu, J., Lin, K., & Ning, C. (2007). Bioinspired structure of bioceramics for bone regeneration in load-bearing sites. *Acta Biomaterialia*, *3*(6), 896–904. doi:10.1016/j.actbio.2007.05.008

Figure Legends

Fig. 1 The experimental geometry: a) stirred tank setup and dimensions; b) detail of the impeller design showing its cylindrical core (arrow).

Fig. 2 a) 3D rendering of the stirred tank; b) 2D view of the computational grid for a 2D axial plane passing through the RP4 impeller blades; c) 3D view of the computational grid generated for the rotating impeller zone (i.e. *radial paddle*), shown in grey.

Fig. 3 Flow field within the stirred tank at 240 rpm. Distributions of the fluid velocity vectors at the axial cross-section of the vessel passing a) in the middle of the RP4 blades and b) through the blades. c) Radial velocity profiles for two sections parallel to the tank bottom, located at 3.5 mm and 10.5 mm above it.

Fig. 4 CFD modelled HA volume fraction distribution in time while stirring. Contour plots in the first line are referred to the $\theta = 0°$ axial cross-section, while those in the second line are referred to the $\theta = 45°$ one.

Fig. 5 Axial distribution of the dimensionless HA volume fraction in time (α/α_{eq}) evaluated for the dimensionless radial coordinate $r^* = 0.5$ belonging to the $\theta = 0°$ axial cross-section. In figure, z/H represents the dimensionless axial coordinate, with $H = 14$ mm.

Fig. 6 Coefficient of variation of the HA volume fraction calculated for the whole stirred tank volume. A stable plateau value of 0.02 is reached after 50 s of mixing, corresponding to the homogenisation time.

Fig 1 (web&print)

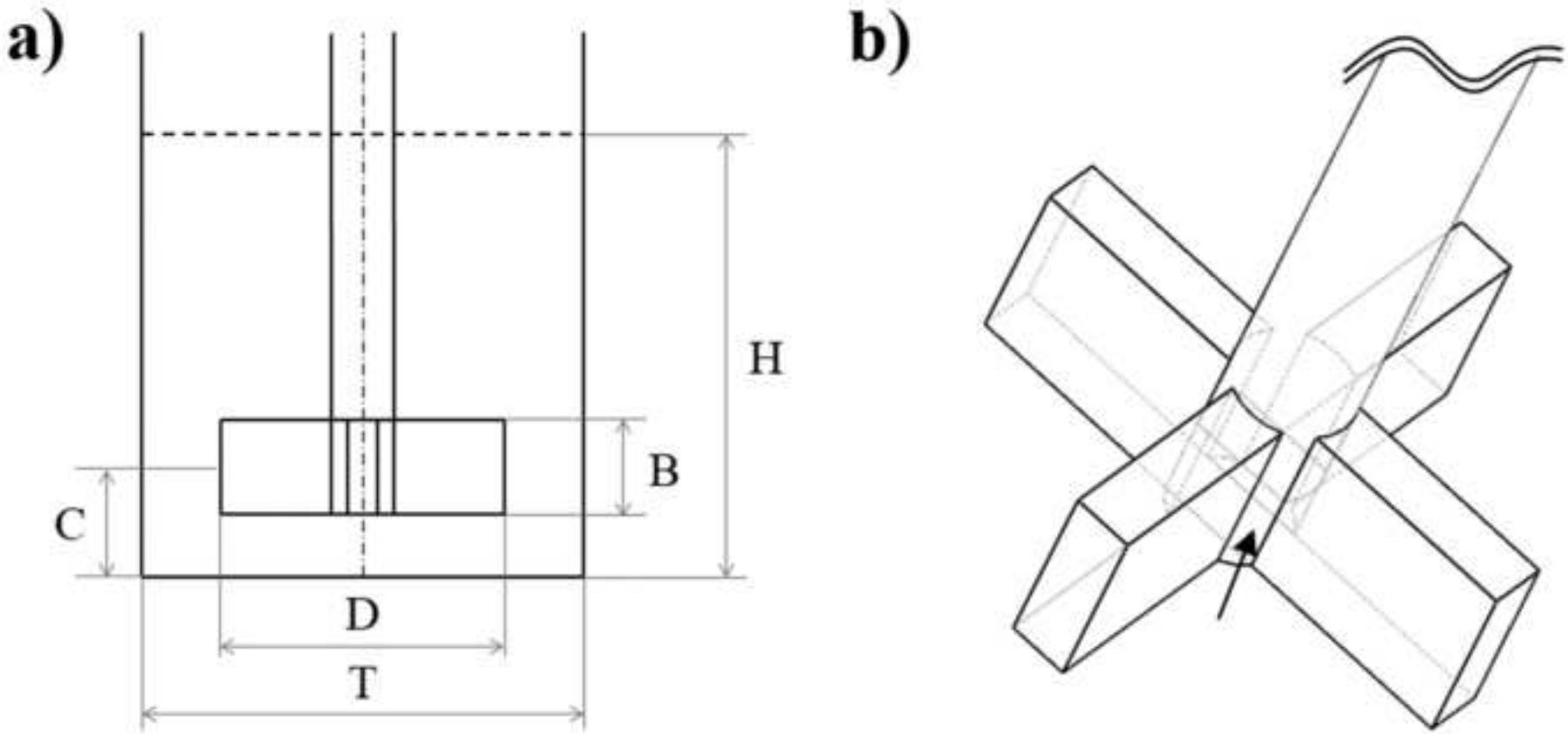

Fig 2 (web&print)

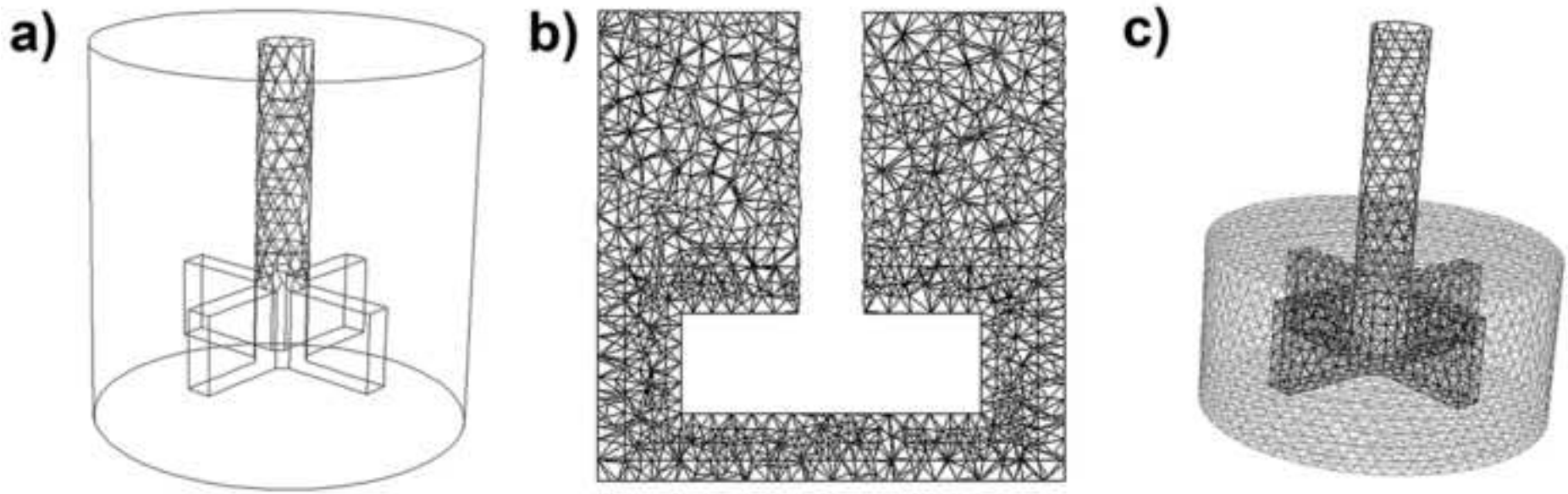

Fig 3 (B&W, print)

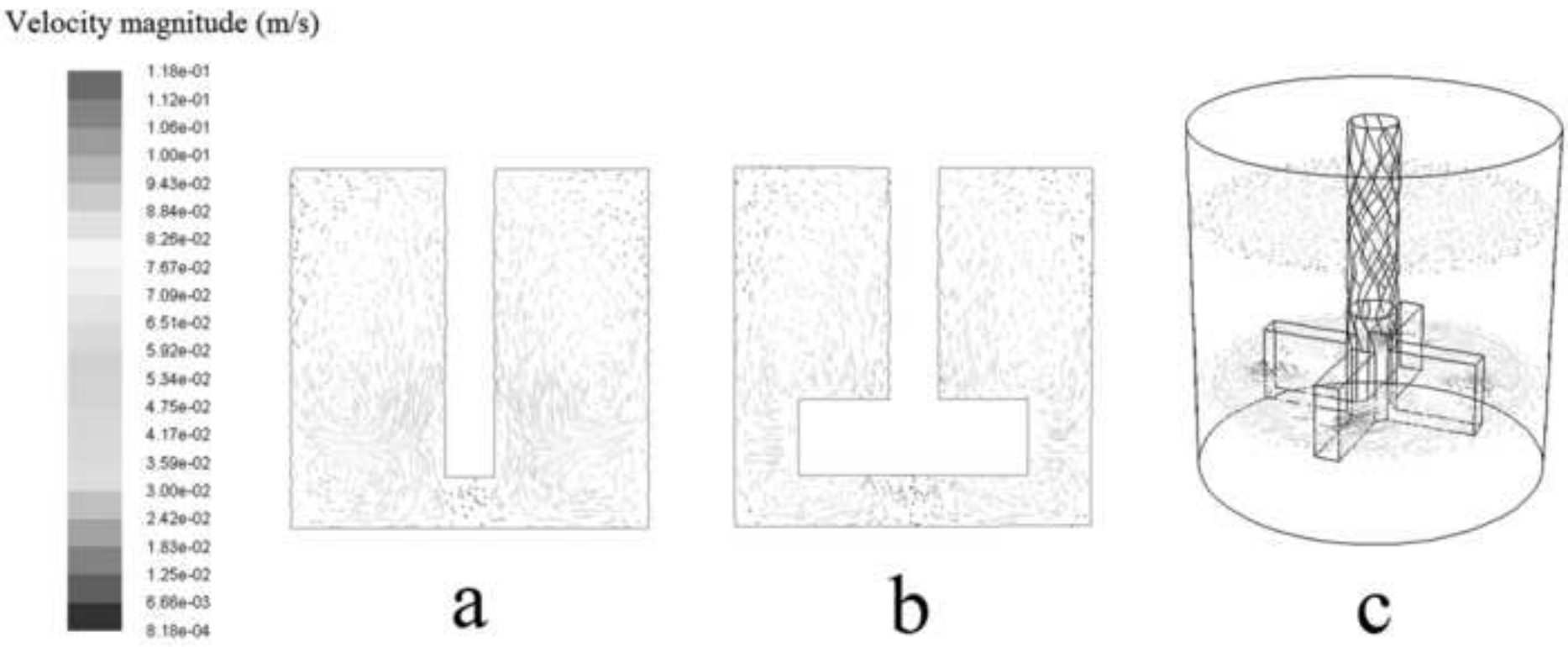

Fig 3 (web)

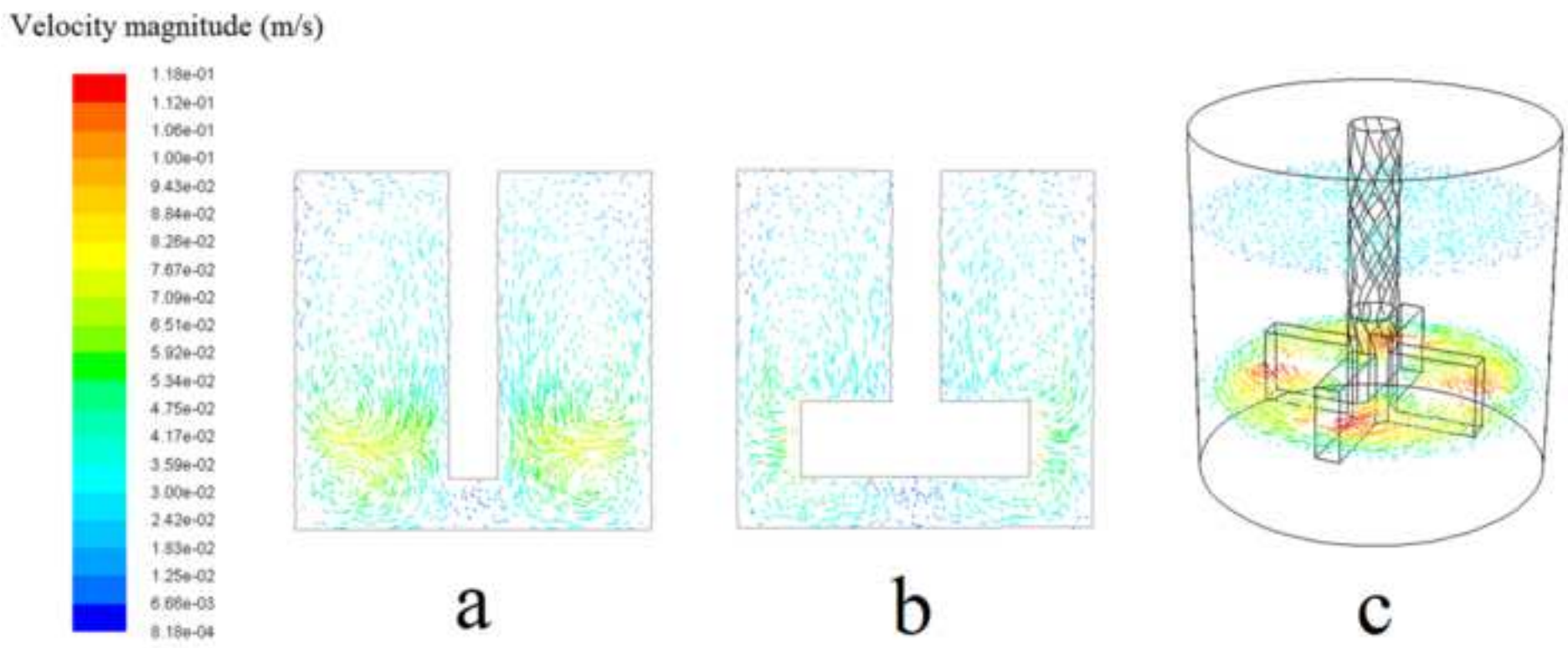
Velocity magnitude (m/s)
1.18e-01
1.12e-01
1.06e-01
1.00e-01
9.43e-02
8.84e-02
8.26e-02
7.67e-02
7.09e-02
6.51e-02
5.92e-02
5.34e-02
4.75e-02
4.17e-02
3.59e-02
3.00e-02
2.42e-02
1.83e-02
1.25e-02
6.68e-03
8.18e-04
a
b
c

Fig 4 (B&W, print)

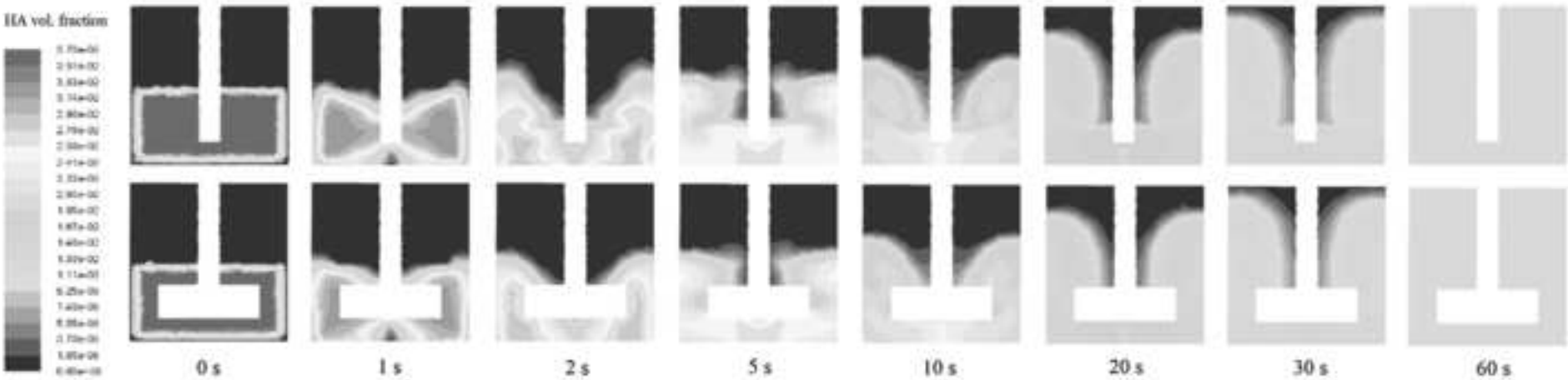

Fig 4 (web)

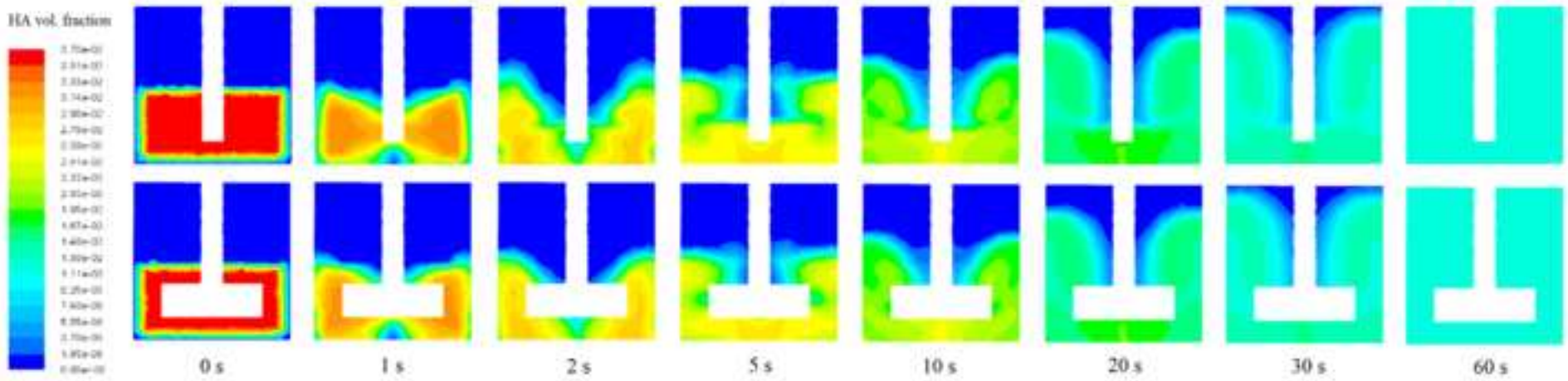

Fig 5 (web&print)

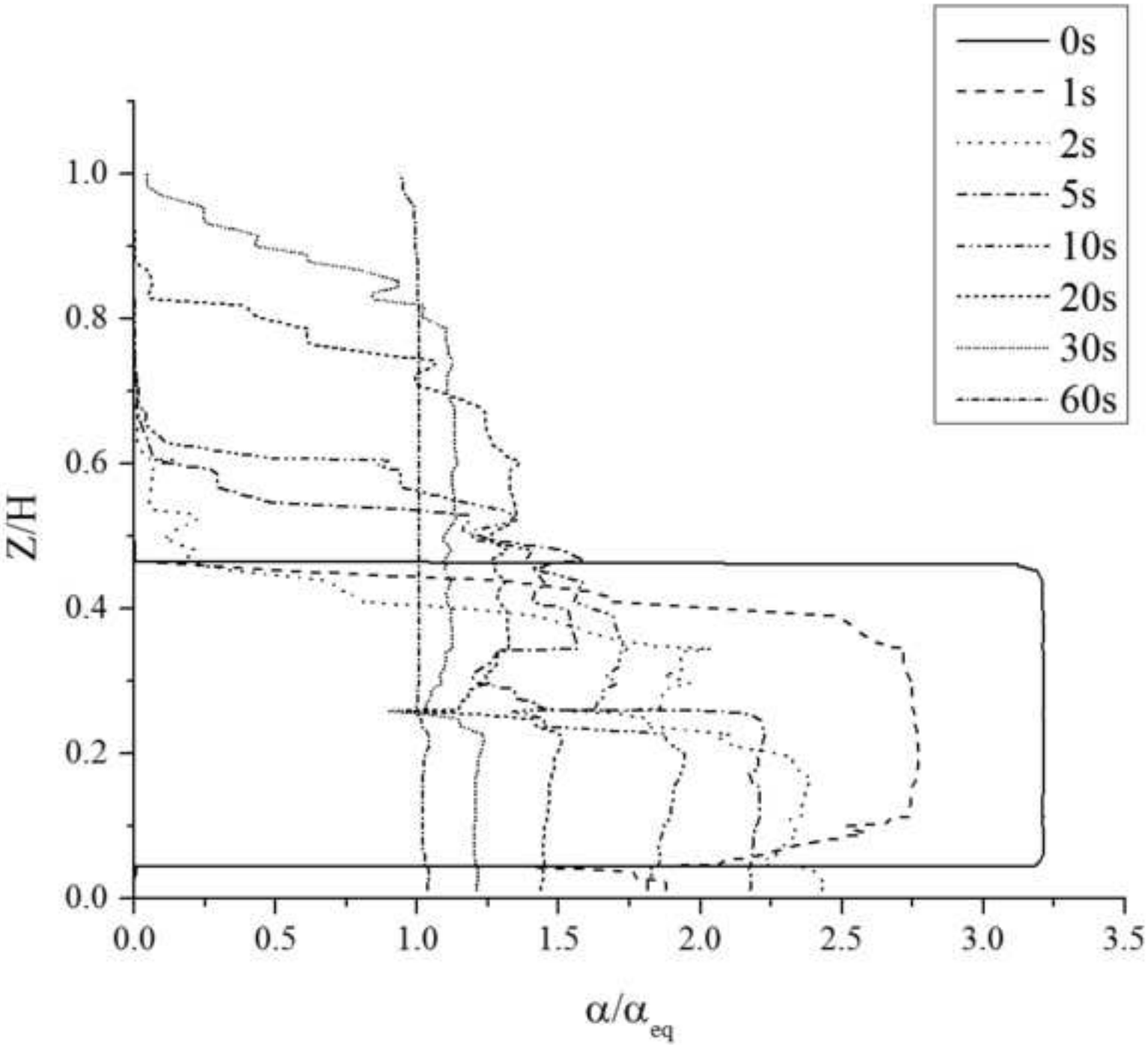

Fig 6 (web&print)